Mono-copper far more active than analogous di-copper complex for electrocatalytic hydrogen evolution

*Varinder Singh, Abdullah M. Abudayyeh, Matthew G. Robb and Sally Brooker**

Department of Chemistry and MacDiarmid Institute for Advanced Materials and Nanotechnology, University of Otago, PO Box 56, Dunedin 9054, New Zealand.

E-mail: sbrooker@chemistry.otago.ac.nz

Electronic Supporting Information

1. Spectroscopic data

1.1 NMR spectra

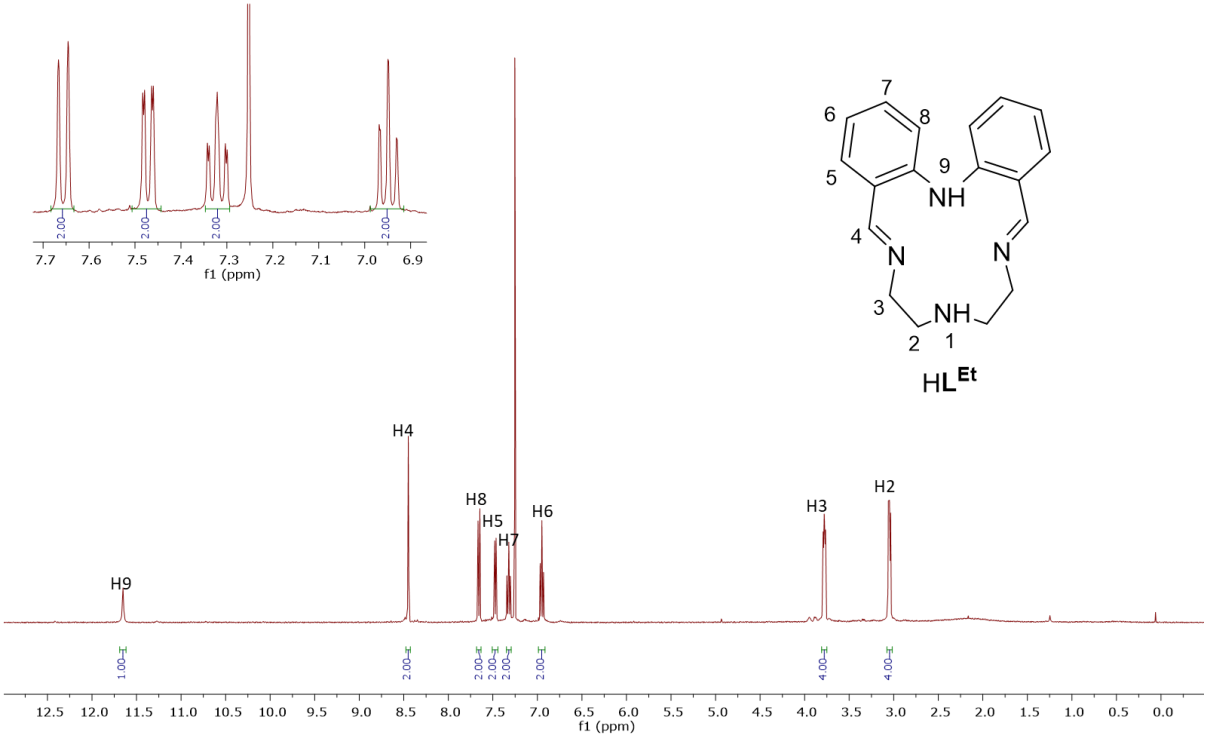

Figure S1. ^{1}H NMR spectrum of the literature macrocyclic ligand, HL^{Et} (400 MHz, $CDCl_3$, 298 K), included here for ease of comparison.[1]

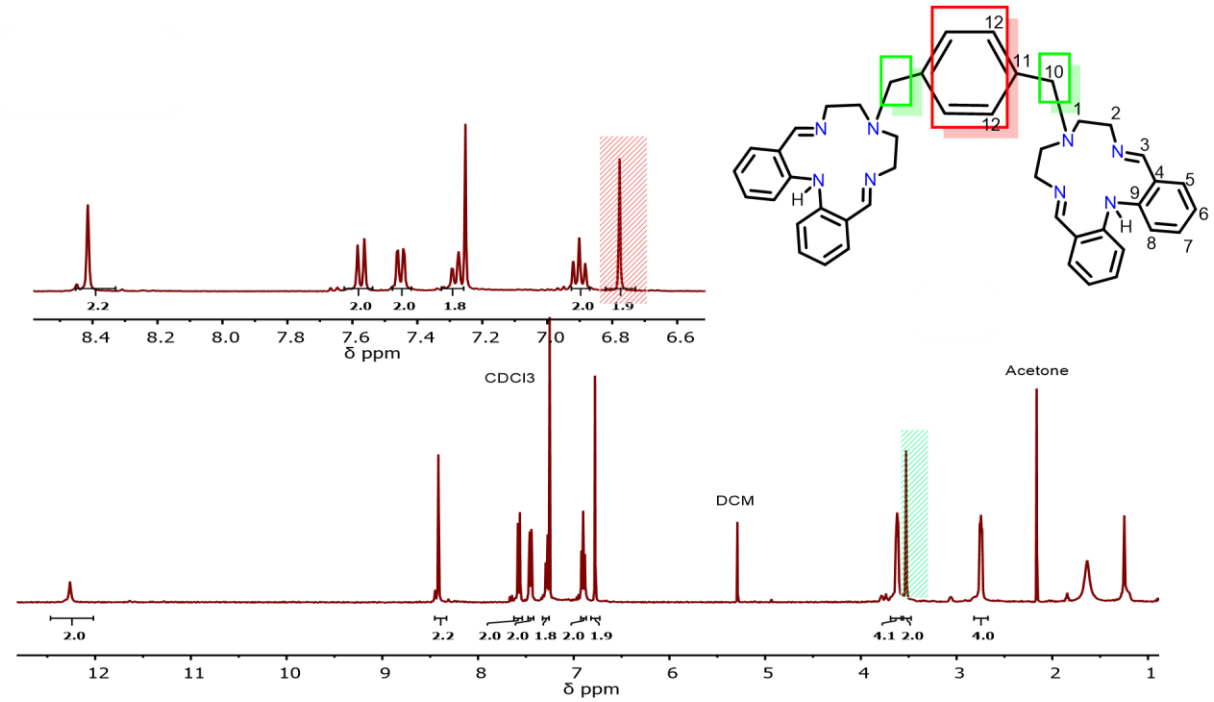

Figure S2. ^{1}H NMR spectrum of bis-macrocyclic ligand, bis-H**L^{Et}** (400 MHz, $CDCl_3$, 298 K). Inset is an expansion of the aromatic region. δ (ppm) = 12.29 (s, 1H, NH), 8.41 (s, 2H, H-3), 7.57 (d, *J* = 8.3 Hz, 2H, H-8), 7.45 (dd, *J* = 7.7, 1.6 Hz, 2H, H-5), δ 7.30 – 7.26 (m, 2H, H-7). 6.90 (td, *J* = 7.5, 1.1 Hz, 2H, H-6), 6.78 (s, 2H, H-12), 3.62 (t, *J* = 5.1 Hz, 4H, H-1), 3.53 (s, 2H, H-10), 2.78 – 2.71 (m, 4H, H-2).

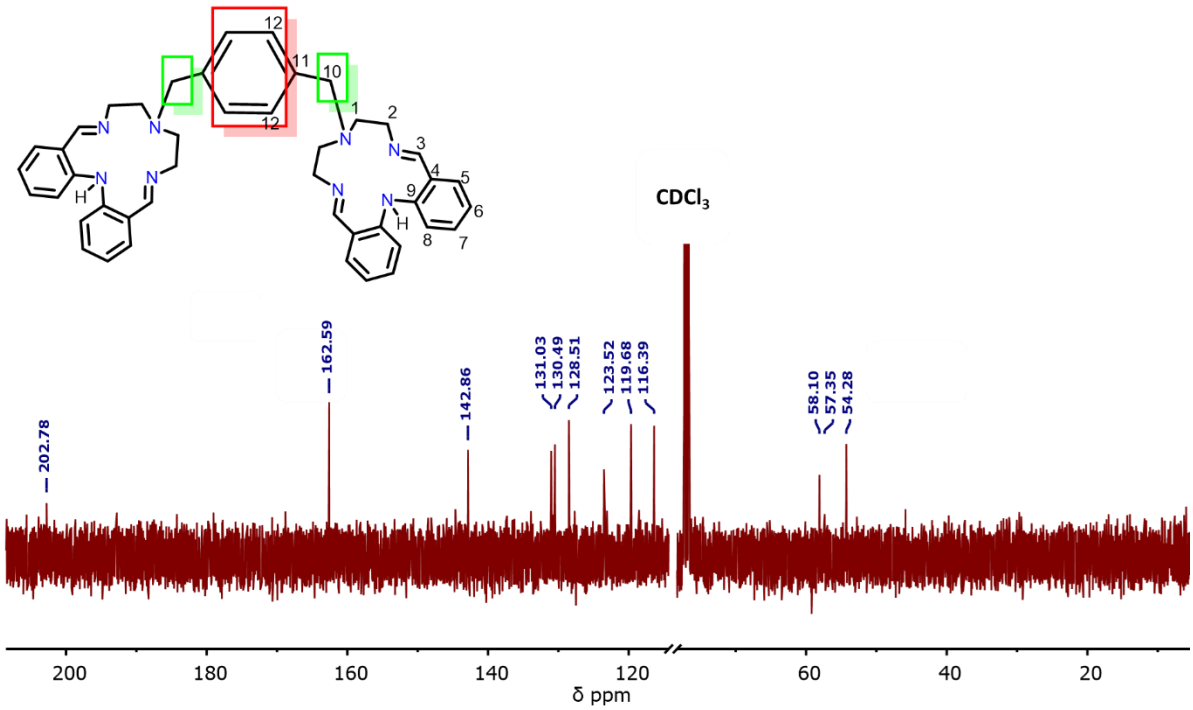

Figure S3. ^{13}C NMR spectrum of bis-macrocyclic ligand, bis-H**L^{Et}** (400 MHz, $CDCl_3$, 298 K). δ (ppm) = 202.78 (C-11), 162.59 (C-3), 142.86 (C-9), 131.03 (C-5), 130.49 (C-7), 128.51 (C-12), 123.52(C-4), 119.68 (C-6), 116.39 (C-8), 58.10 (C-1), 57.35 (C-2), 54.28 (C-10).

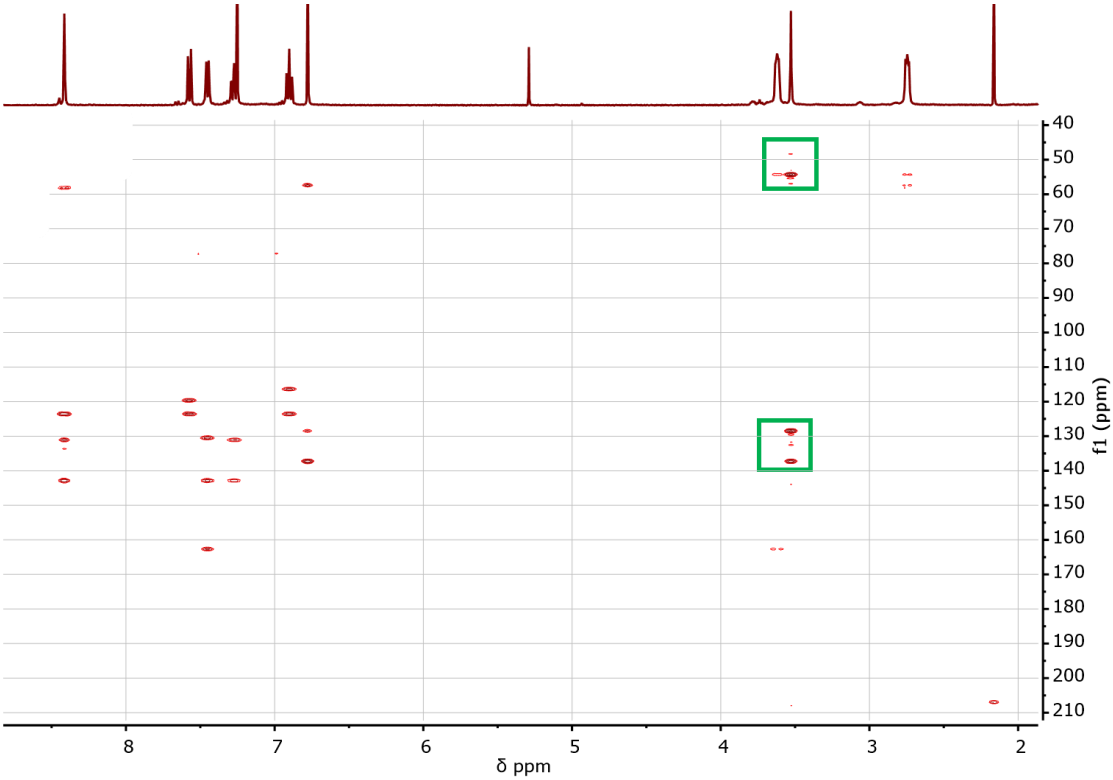

Figure S4. HMBC NMR spectrum of bis-macrocyclic ligand, bis-H**L**^{Et} (400 MHz, $CDCl_3$, 298 K).

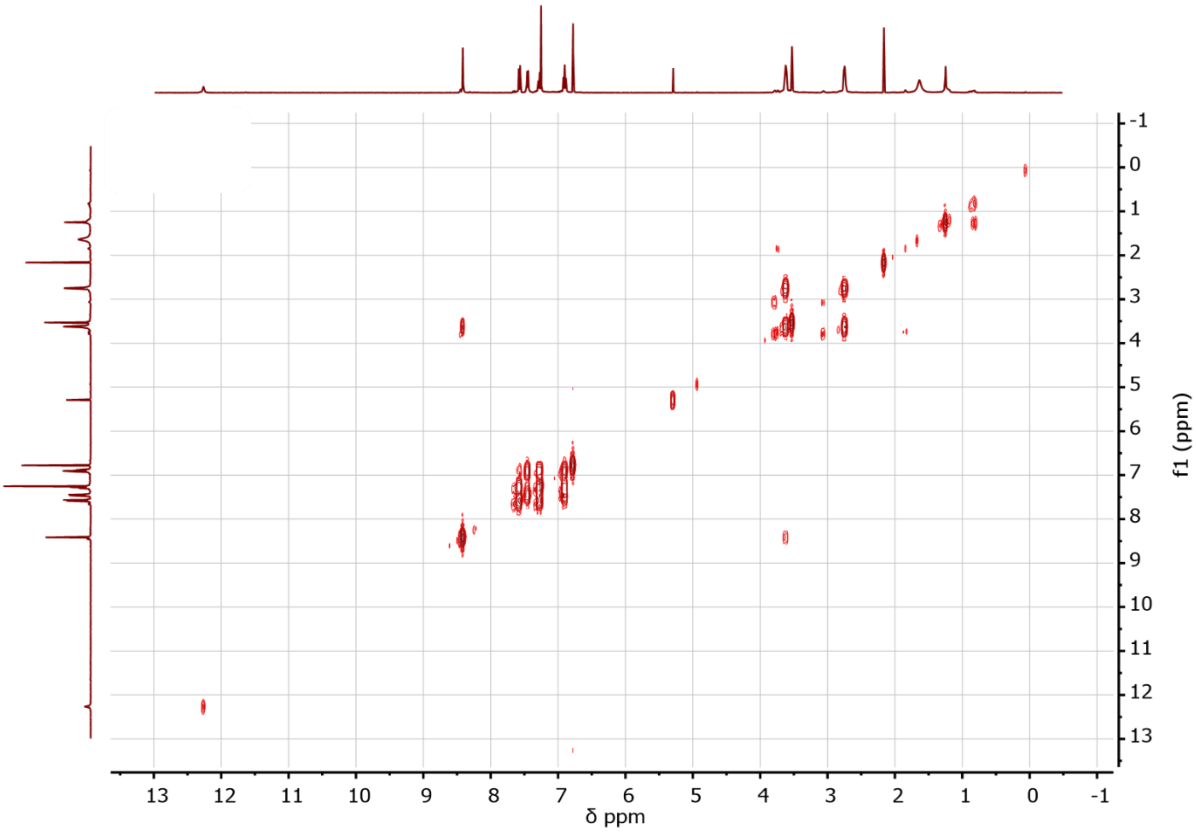

Figure S5. COSY NMR spectrum of bis-macrocyclic ligand, bis-H**L**^{Et} (400 MHz, $CDCl_3$, 298 K).

1.2 ESI-Mass spectra

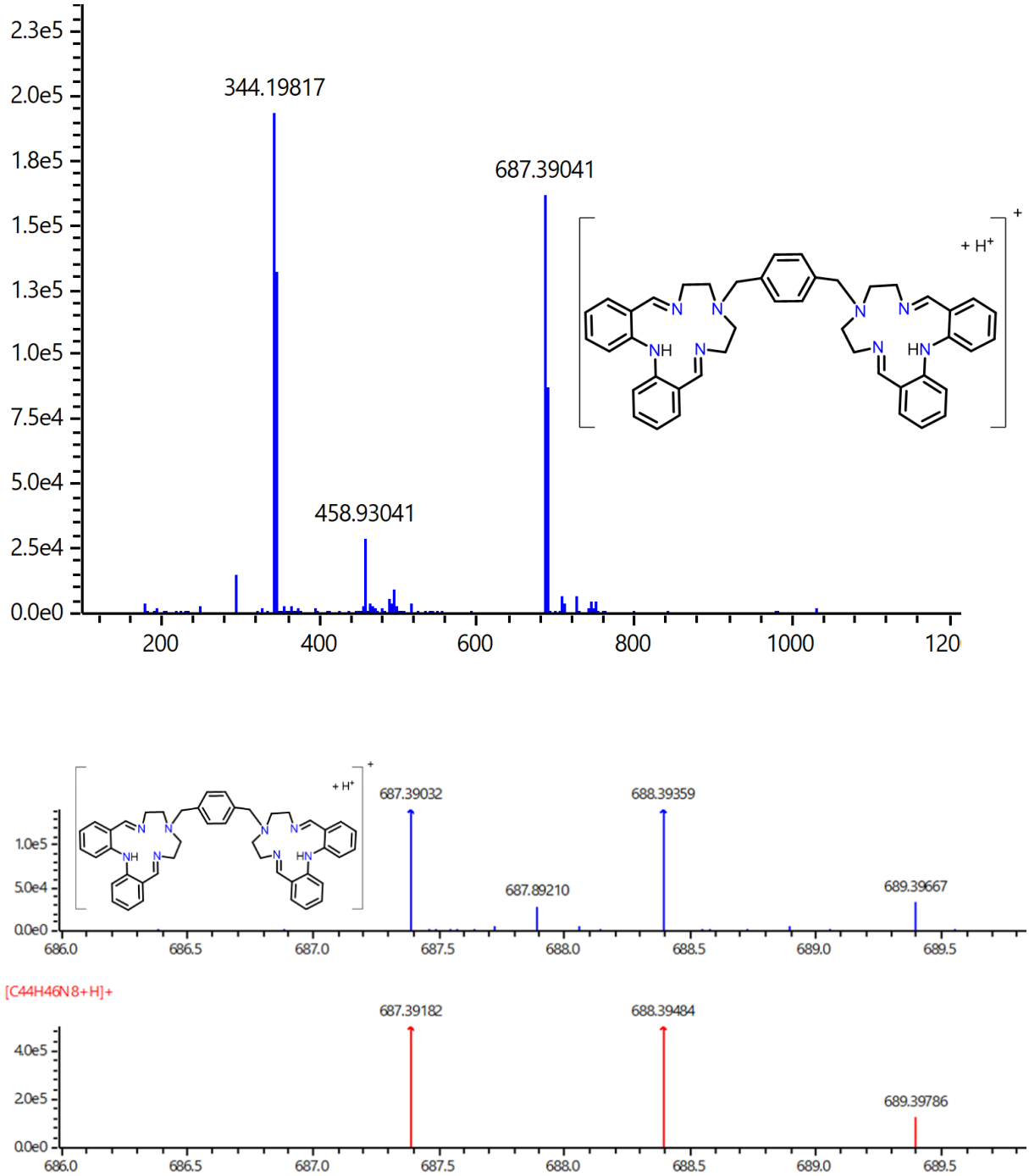

Figure S6. (Top) Mass spectrum (MS-ESI-positive mode) of bis-macrocyclic ligand, bis-H**L**^{Et}; (bottom) actual and simulated spectrum for the peak corresponding to the [**bis**-H**L**^{Et} + H]$^+$ = $(C_{44}H_{46}N_8+H)^+$ ion.

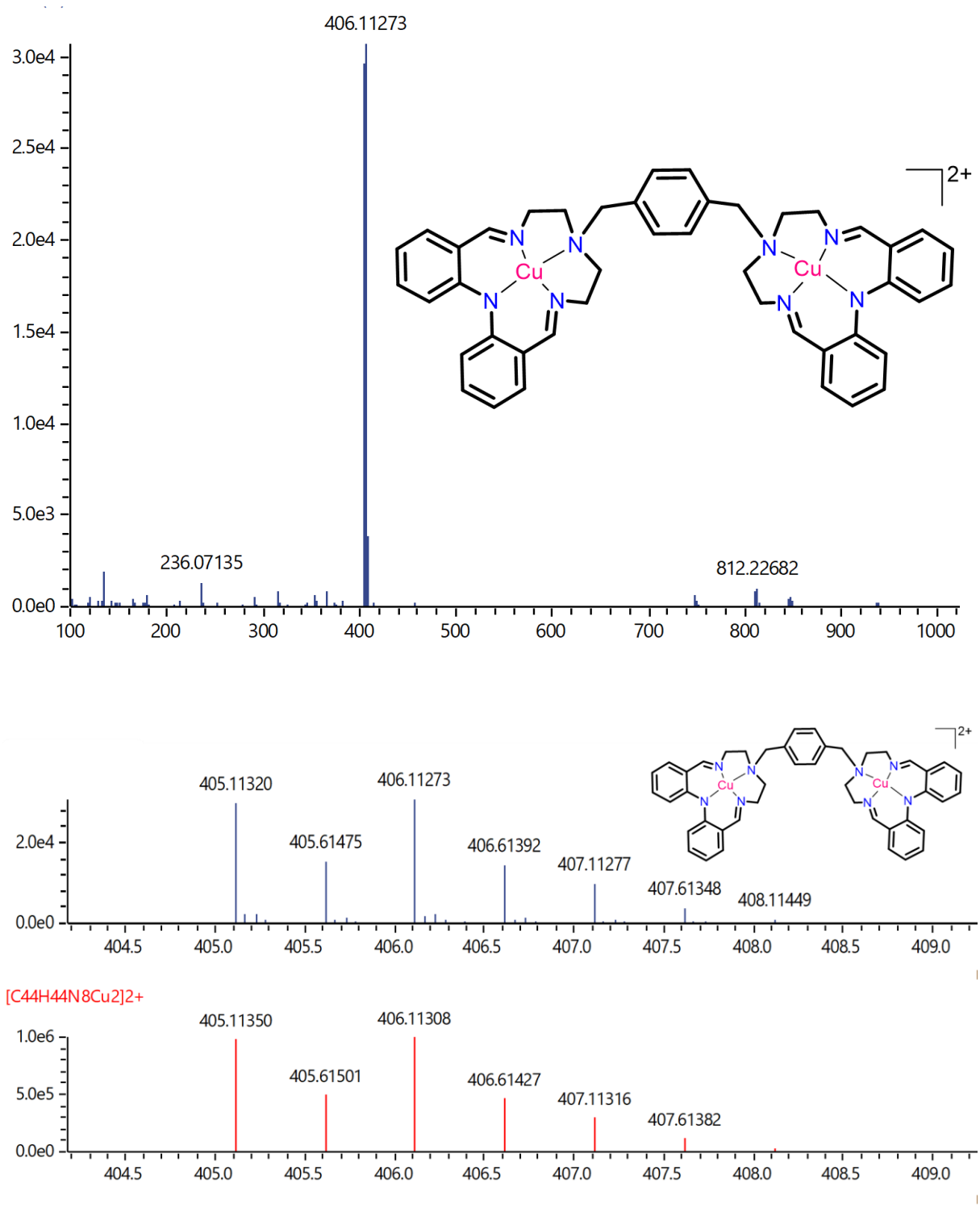

Figure S7. (top) Mass spectrum (MS-ESI-positive mode) of bis-macrocyclic copper complex **2**, $[Cu^{II}_2(\textbf{bis-L}^{Et})](BF_4)_2$; (bottom) actual and simulated spectra for the peak corresponding to the $[Cu^{II}_2(\textbf{bis-L}^{Et})]^{2+} = (C_{44}H_{44}N_8Cu_2)^{2+}$ ion.

1.3 X-ray crystallography

X-ray crystallographic data was collected on an Oxford Diffraction SuperNova diffractometer with Atlas CCD, equipped with a Cryostream N_2 open-flow cooling device, using mirror monochromated micro-focus Cu-*Kα* (1.54 Å) radiation at 100 K. A complete set of unique reflections to a maximum resolution of 0.82 Å was collected. Raw frame data (including data reduction, inter-frame scaling, unit cell refinement and absorption corrections) were processed using *CrysAlis Pro.*[2] The structure was solved and refined against all F^2 data using *SHELXL-2014.*[3] *OLEX2*[4] was used as the interface to visualise the structure during the refinement process. All non-H atoms were refined anisotropically. Hydrogen atoms were inserted at calculated positions with U(H) = 1.2 U(attached atom). High resolution pictures were prepared using Mercury[5] and POVray[6] software.

Yellow brown pointed block shaped crystals of **[Cu^{II}_2(bis-L^{Et})](BF_4)$_2$**·2CH_3CN (**2**·2CH_3CN, Figure S8, left) were obtained as detailed in the experimental section.

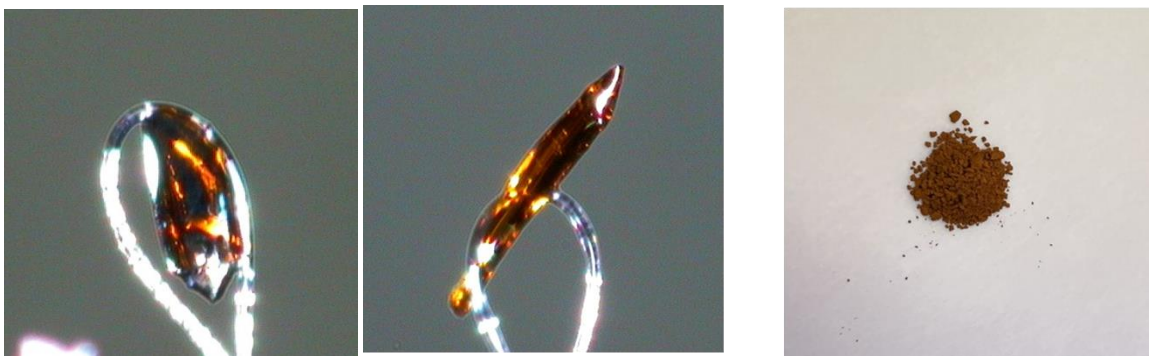

Figure S8. The dicopper(II) bis-macrocyclic complex, Cu^{II}_2(**bis-L^{Et}**)](BF_4)$_2$ (**2**) prepared herein as a: (left) single crystals of **2**·2MeCN (left one used for the data collection reported herein), and (right) powder of **2**·4H_2O.

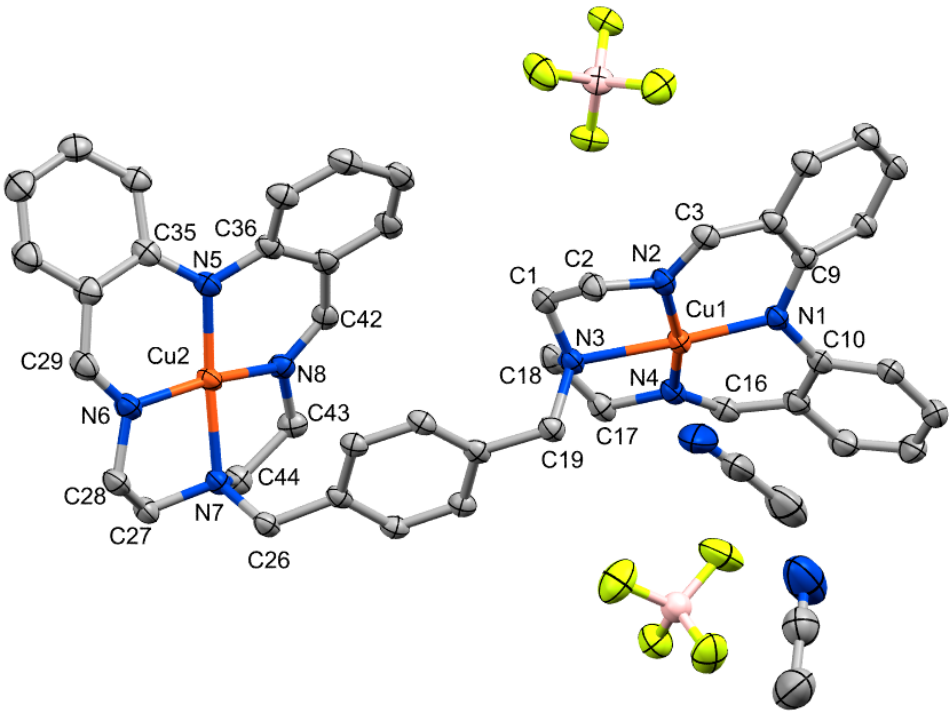

Figure S9: The asymmetric unit of X-ray crystal structure (shown as 50% ellipsoids) of $[Cu^{II}_2(\textbf{bis-L}^{Et})](BF_4)_2\cdot 2MeCN$, including the 2 counter ions (one of which is disordered over 2 overlapping sites, 85:15, SAME used to optimise geometry of both sets using the non-disordered anion; not shown) and 2 full occupancy MeCN solvent molecules.

Table S1. Crystal data and structure refinement details for the bis-macrocyclic complex **2**·2CH_3CN $[Cu^{II}_2(\textbf{bis-L}^{Et})](BF_4)_2$·2$CH_3CN$

	$[Cu^{II}_2(\textbf{bis-L}^{Et})](BF_4)_2$·2$CH_3CN$ (**2**·2CH_3CN)
Empirical formula	$C_{48}H_{50}B_2Cu_2F_8N_{10}$
M_r	1067.68
Crystal system	triclinic
Space group	P-1
a [Å]	9.3827(2)
b [Å]	13.8186(4)
c [Å]	18.5659(5)
α [°]	77.963(2)
β [°]	84.825(2)
γ [°]	80.221(2)
V [Å^3]	2322.42(11)
Z	2
T [K]	100
$\rho_{calcd.}$ [g/cm^3]	1.527
μ [mm^{-1}]	1.816
F(000)	1096.0
Crystal Size (mm)	0.484 × 0.215 × 0.102
2θ range for data collection	7.392 to 145.642
Reflections collected	42909
Independent reflections	9116
R(int)	0.0393
Data / restraints / parameters	9116/30/668
Goof (F^2)	1.026
R_I [I>2σ(I)]	0.0422
wR_2 [all data]	0.1802
Max/min res. e density [eÅ^{-3}]	0.85 and -0.41

Table S2. Selected bond lengths [Å] and angles (°) for **1**, [Cu^{II}**L^{Et}**](BF_4) reported previously in Ref [1].

Bond Length [Å]	
Cu-N_{dpa} (Cu1-N1)	1.932(5)
Cu-N_{imine} (Cu1-N2/N4)	1.898(6)/1.932(6)
Cu-N_{amine} (Cu1-N3)	2.036(6)
Bond Angle [°]	
N(2)-Cu(1)-N(1)	96.4(2)
N(2)-Cu(1)-N(4)	166.2(2)
N(1)-Cu(1)-N(4)	96.1(2)
N(2)-Cu(1)-N(3)	83.6(2)
N(4)-Cu(1)-N(3)	84.0(2)
N(1)-Cu(1)-N(3)	179.3(3)

Table S3. Selected bond lengths [Å] and angles (°) for **2**·2CH_3CN [Cu^{II}(**bis**-**L^{Et}**)](BF_4)$_2$·2CH_3CN.

Bond Length [Å]	
Cu-N_{dpa} (Cu1-N1; Cu2-N5)	1.939(2); 1.928(2)
Cu-N_{imine} (Cu1-N2/N4; Cu2-N6/N8)	1.908(2)/1.921(2); 1.913(2), 1.911(2)
Cu-N_{amine} (Cu1-N3; Cu2-N7)	2.103(2); 2.052(2)
Bond Angle [°]	
N(2)-Cu(1)-N(1)	95.5(9)
N(2)-Cu(1)-N(4)	165.5(9)
N(1)-Cu(1)-N(4)	95.2(9)
N(2)-Cu(1)-N(3)	84.7(8)
N(4)-Cu(1)-N(3)	83.9(8)
N(1)-Cu(1)-N(3)	176.3(8)
N(5)-Cu(2)-N(7)	174.9(9)
N(6)-Cu(2)-N(5)	95.1(1)
N(6)-Cu(2)-N(7)	85.7(9)
N(6)-Cu(2)-N(8)	166.2(1)
N(8)-Cu(2)-N(5)	95.7(9)
N(7)-Cu(2)-N(8)	84.1(8)

2. Electrochemistry and electrocatalytic HER

General method: All electrochemical measurements were carried out in a three neck H-shaped electrochemical cell under an argon atmosphere (all solutions were purged with Ar for 20-30 min prior to study), using an IVIUMSATT.XRE potentiostat, a glassy carbon (3 mm diameter, surface area = 0.071 cm^2) as the working electrode, 0.01 M $AgNO_3$/Ag as the reference electrode, platinum sheet as the counter electrode. The working electrode compartment was filled with 8 mL of 0.1 M Bu_4NPF_6 acetonitrile solution, and the rest of the "H" was filled with ca. 10 mL of 0.1 M Bu_4NPF_6 acetonitrile solution. Ferrocene was used as an internal reference check.

Acetonitrile was freshly distilled over calcium hydride. Bu_4NPF_6 (99 %, for electrochemical analysis) was purchased from Sigma Aldrich and used without further purification.

The working electrode was cleaned before each measurement by: rinsing with water, ethanol and acetonitrile, then polishing with alumina slurry, and finally rinsing with acetonitrile and drying.

The three neck H-shaped electrochemical cell and Pt counter electrode were carefully cleaned and dried between studies as follows: filled and soaked in nitric acid (1 hour), rinsed thoroughly with copious water, filled and soaked in water (2 hours), rinsed with water, acetonitrile and acetone, soaked in dry MeCN for 24 hours, emptied and dried in an oven overnight before use.

Cyclic Voltammetry (CV): CVs where carried out on 8 mL acetonitrile solutions that were 1 mM in **1**, **2**·$4H_2O$ or the salt $Cu^{II}(BF_4)_2 \cdot xH_2O$, and 0.1 M in Bu_4NPF_6. An internal reference check to the ferrocene/ferrocenium cation couple ($Fc^{+/0}$) was carried out at the conclusion of every study, and was consistently observed at $E_{1/2}$ = 0.09 ± 0.01 V, with ΔE = 0.09 V, vs 0.01 M $AgNO_3$/Ag. Prior to each study, the purity of the electrolyte and solvent and the cleanliness of the cell setup was first checked by recording the CV from 0 to 2.0 to -2.0 to 0 V to confirm negligible background current was observed, before adding the respective copper complex and commencing the study.

Controlled Potential Electrolysis (CPE): CPE measurements were conducted using same cell described above, but in this case the working compartment was filled with 8 mL of 0.1 M Bu_4NPF_6 acetonitrile solution containing the specified amount of acid (0.08 M unless otherwise stated) and 1 mM in the copper complex. The remainder of the 'H' was filled with ca. 10 mL of 0.1 M Bu_4NPF_6 acetonitrile solution. Glassy carbon electrode (0.071 cm^2) and the 0.01 M $AgNO_3$/Ag reference electrode were placed into the working compartment, and the Pt sheet counter electrode was placed in the auxiliary compartment.

Additional reference electrode checks: The check was done by taking the reference electrode out, rinsing it and placing it into a separate electrochemical cell containing 1 mM ferrocene in the same electrolyte solution and running the CV. These checks on the reference electrode, before and after CVs and CPE experiments on **2**·$4H_2O$ with acid present, showed that no drift occurred during these experiments, as $E_{1/2}(Fc^+/Fc)$ = 0.09 ± 0.01 V vs 0.01 M $AgNO_3$/Ag, with ΔE = 0.09 ± 0.01 V, in all cases (Figure S11).

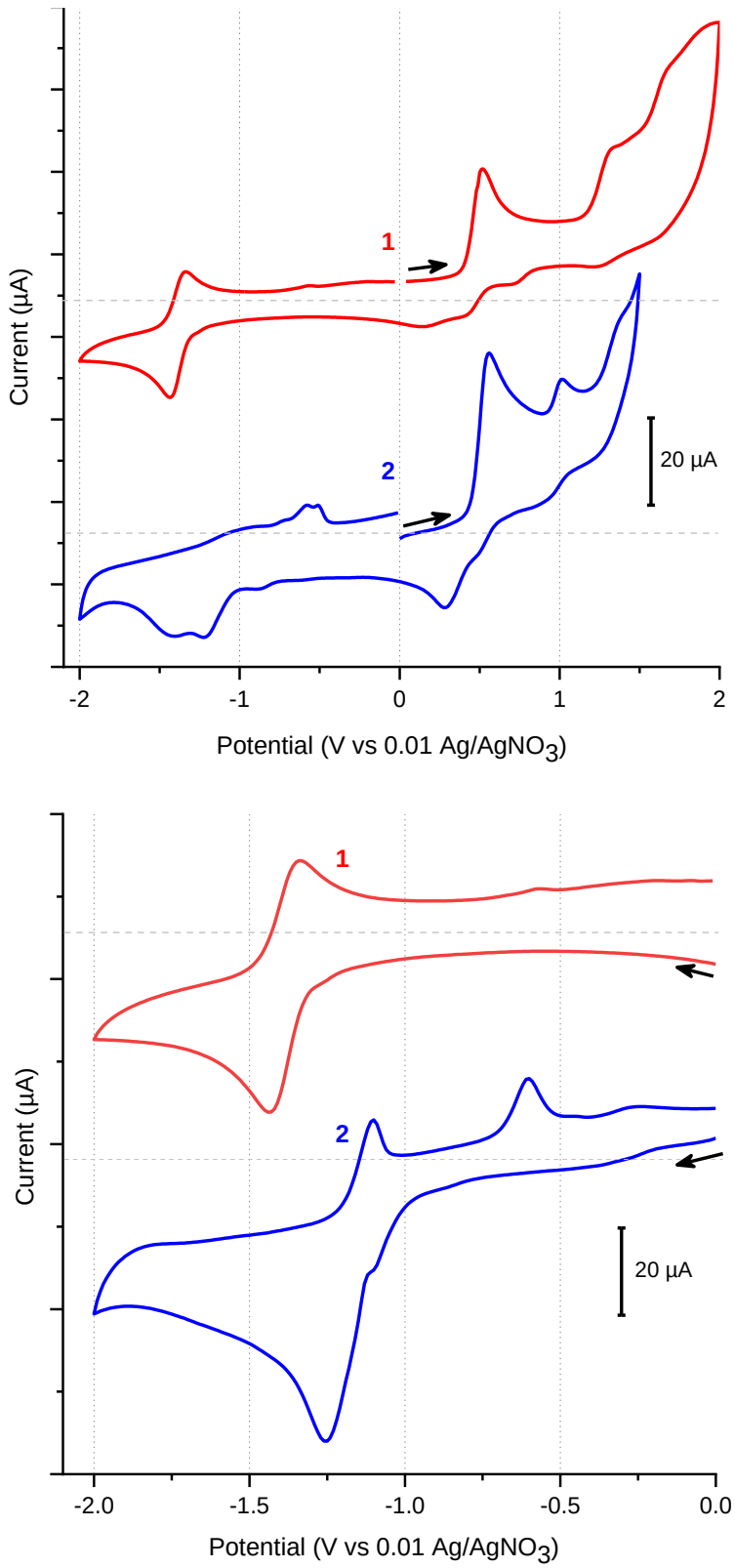

Figure S10. (Top) Full range CVs (E = 0→ +2→ 0→ -2→ 0 V) and (bottom) cathodic range CVs (E = 0→ -2→ 0 V) of an acetonitrile solution of 1 mM (blue) **1** $[Cu^{II}\mathbf{L^{Et}}]BF_4$ (already published[7] but included here for ease of comparison) and (red) **2**·$4H_2O$ $[Cu^{II}(\mathbf{bis\text{-}L^{Et}})](BF_4)_2 \cdot 4H_2O$. The CVs were collected vs 0.01 M $AgNO_3$/Ag, using 0.1 M $(Bu_4N)_4PF_6$ electrolyte, 3 mm glassy carbon (A = 0.071 cm^2 working electrode, scan rate of 100 mV/s and temperature of 20°C. Internal reference check $E_{1/2}(Fc^+/Fc)$ = 0.09 ± 0.01 V vs 0.01 M $AgNO_3$/Ag, with ΔE = 0.09 ± 0.01 V.

Table S4. Electrochemical parameters extracted form cyclic voltammetry data on complexes **1** (already published[7] but included here for ease of comparison) and **2**·$4H_2O$, at different scan rates (Figure 3). Conditions: 0.1 M $(Bu_4N)PF_6$, glassy carbon working electrode (d = 3 mm, A = 0.071 cm^2), 293 K, vs 0.01 M $AgNO_3$/Ag.

complex	Scan rate (mV/s)	E_c (V)	E_a (V)	$E_{1/2}$ (V)	ΔE (V)	i_c (μA)	i_a (μA)	I_a/i_c
1	50	-1.43	-1.34	-1.39	0.09	-14.7	14.1	1.0
	100	-1.43	-1.34	-1.39	0.09	-18.9	18.5	1.0
	200	-1.43	-1.34	-1.39	0.09	-27.6	27.8	1.0
	400	-1.43	-1.34	-1.39	0.09	-41.4	39.7	1.0
2·$4H_2O$	50	-1.11	-1.26	-1.19	0.15	15.1	15.2	1.0
	100	-1.11	-1.26	-1.19	0.15	28.2	23.8	0.8
	200	-1.14	-1.26	-1.20	0.12	32.3	34.0	1.0
	400	-1.14	-1.26	-1.20	0.12	47.6	50.1	1.1
	600	-1.14	-1.26	-1.20	0.12	58.2	60.2	1.0
	800	-1.14	-1.26	-1.20	0.12	68.4	70.1	1.0
	1000	-1.14	-1.26	-1.20	0.12	76.8	81.1	1.1

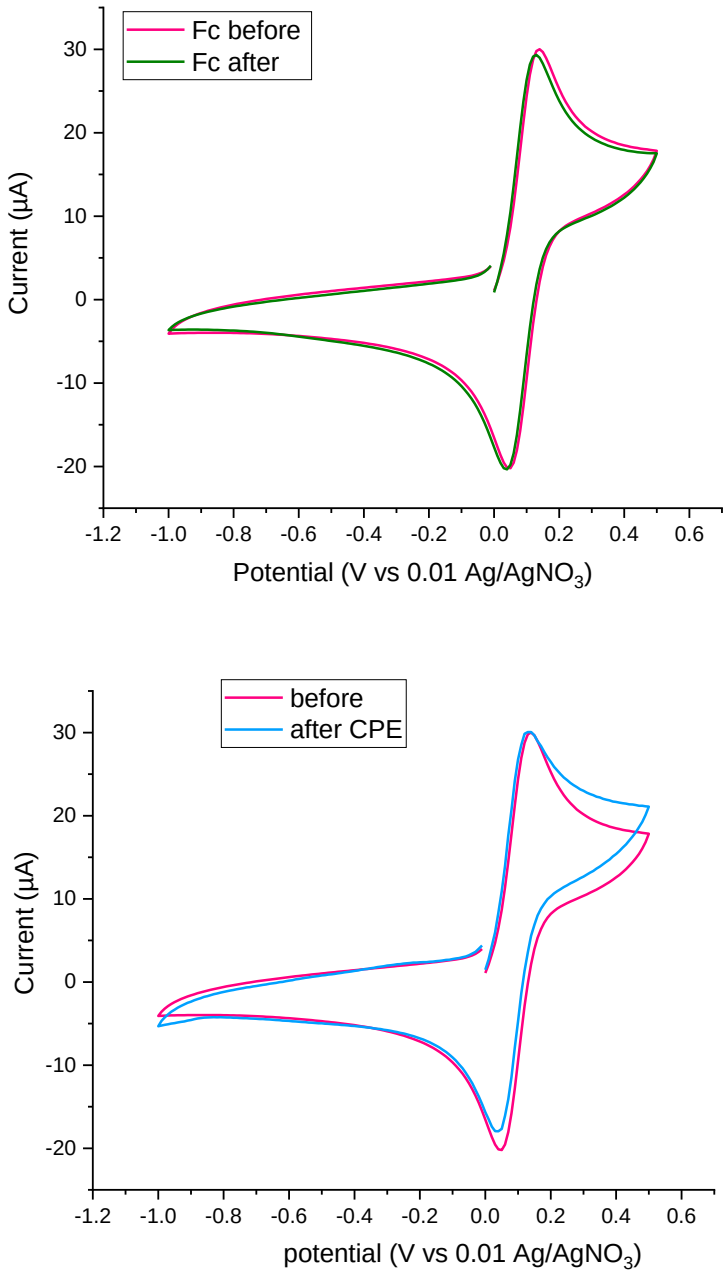

Figure S11. The before and after reference checks (details above) to prove there is no drift (top) before and after collecting CVs and (bottom) before and after CPE experiments, on **2**·$4H_2O$: $E_{1/2}(Fc^+/Fc)$ = 0.09 ± 0.01 V vs 0.01 M $AgNO_3$/Ag, with ΔE = 0.09 ± 0.01 V. Conditions: 0.1 M $(Bu_4N)PF_6$, 3 mm glassy carbon working (A = 0.071 cm^2) and Pt counter electrode, 100 mV/s, 20°C.

To calculate the diffusion coefficient, *D*, the Randles–Sevcik equation[8] is:

$$i_p \quad = 0.4463nFAC^0\left(\frac{nF\upsilon D}{RT}\right)^{\frac{1}{2}} \qquad (1)$$

Where

i_p is the peak current (A),

n is number of electrons transferred,

A is electrode surface area (cm^2),

C^0 is analyte concentration (mol cm^{-3}),

υ is scan rate (V/s),

D is diffusion coefficient (cm^2 s^{-1}),

F is Faraday's constant (C mol^{-1}),

R is gas constant (J K^{-1} mol^{-1}) and

T is temperature (K).

Rearranging eqn 1 slightly gives:

$$i_p \quad = \left[0.4463nFAC^0\left(\frac{nFD}{RT}\right)^{1/2}\right]\upsilon^{\frac{1}{2}}$$

So the slope of a plot of $i_p$versus $\upsilon^{\frac{1}{2}}$ is given by:

$$slope \quad = 0.4463nFAC^0\left(\frac{nFD}{RT}\right)^{\frac{1}{2}} \qquad (2)$$

Enabling easy calculation of *D* the diffusion coefficient from the slope by rearranging eqn 2:

$$D \ = \left(\frac{slope}{0.4463nFAC^0}\right)^2\frac{RT}{nF}$$

Then substituting n = 2, A = 0.071 cm^2, C^0 = 1x10^{-6} (mol cm^{-3}), F = 96,485 (C mol^{-1}), R = 8.314(J K^{-1} mol^{-1} and T = 293 K:

$$\underline{D \ = 338\ (slope)^2 \ \ cm^2s^{-1}}$$

For **2**·4H_2O, [Cu^{II}(Bis-$\mathbf{L^{Et}}$)](BF_4)$_2$·4H_2O

Equation of best fit line in plot of $i_p$versus $\upsilon^{\frac{1}{2}}$ (Figure S12) is: y = $1.82x10^{-6}$– $78x10^{-6}$X

i.e. slope = -$78x10^{-6}$ A $V^{1/2}$

Giving D = 338 $(-78x10^{-6})^2 = \ 2.05x10^{-6}$$cm^2s^{-1}$

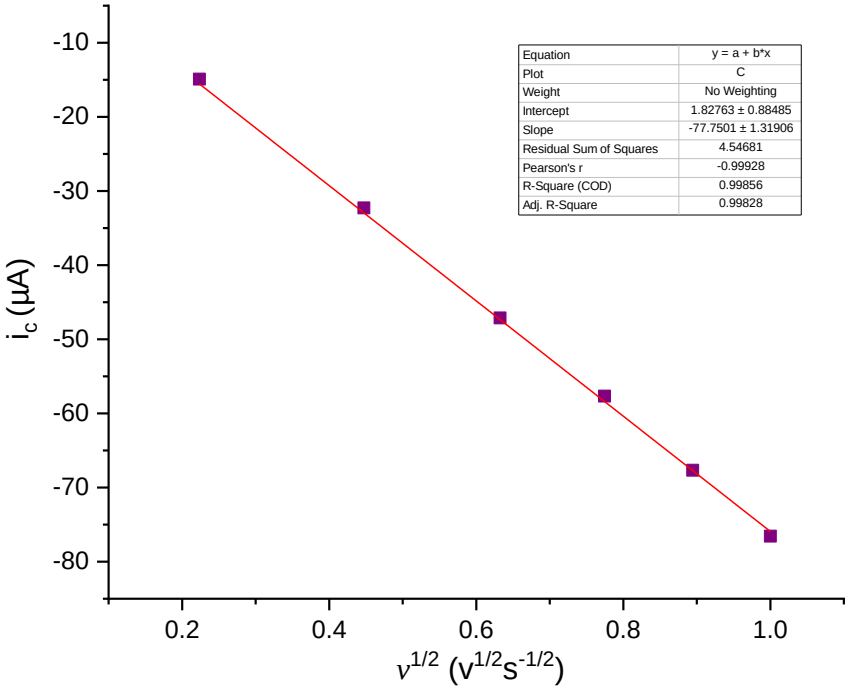

Figure S12. Plot of catholic peak current versus the square root of the scan rate ($\boldsymbol{\upsilon}^{1/2}$) of the reversible redox event for 1 mM acetonitrile solution of dicopper complex **2**·4H_2O, [Cu^{II}(**Bis-L^{Et}**)](BF_4)$_2$·4H_2O (E_{pc} = -1.26 V). Diffusion coefficient (*D*) = 2.05×10^{-6} cm^2 s^{-1}. Conditions: Electrolyte; 0.1 M (Bu_4N)PF_6, working electrode; 3 mm glassy carbon (A = 0.071 cm^2), 20° C. R^2 = 0.999, slope = -78 x 10^{-6}, intercept = 1.8 µA.

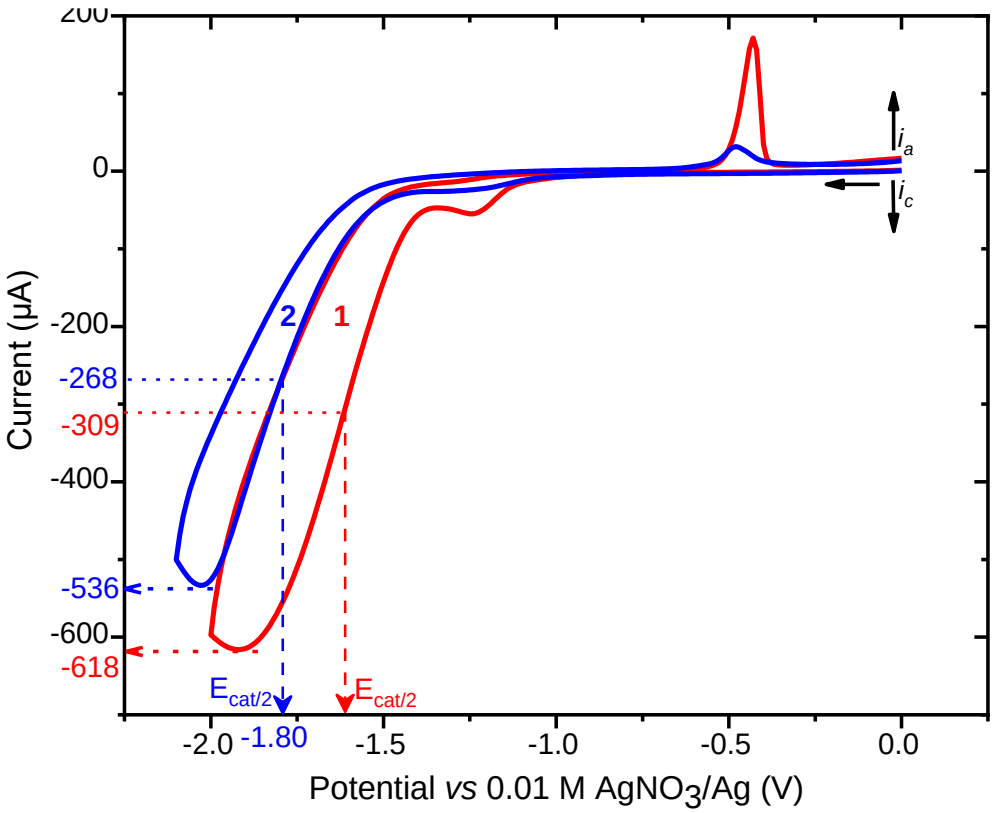

Figure S13. CV of 80 mM acetic acid in MeCN solution (1mM) of (red) monocopper complex **1** and (blue) dicopper complex **2**·4H_2O, the figure shows how the potential at half of the catalytic current, $E_{cat/2}$,[ref9] was obtained for each complex. Conditions: Electrolyte; 0.1 M (Bu_4N)PF_6, working electrode; 3 mm glassy carbon (A = 0.071 cm^2), 20°C.

References

1. Sanyal, R.; Cameron, S. A.; Brooker, S., Synthesis and complexes of an N_4 Schiff-base macrocycle derived from 2,2'-iminobisbenzaldehyde. *Dalton Trans.* **2011,** *40*, 12277-12287.
2. *CrysAlisPro*, CrysAlisPro, Version 171.37.33; Agilent Technologies: Yarnton, Oxfordshire, **2014**.
3. Sheldrick, G., Crystal structure refinement with SHELXL. *Acta Crystallogr., Sect. C* **2015,** *71* (1), 3-8.
4. Dolomanov, O. V.; Bourhis, L. J.; Gildea, R. J.; Howard, J. A. K.; Puschmann, H., OLEX2: a complete structure solution, refinement and analysis program. *J. Appl. Cryst.* **2009,** *42*, 339-341.
5. Macrae, C. F.; Bruno, I. J.; Chisholm, J. A.; Edgington, P. R.; McCabe, P.; Pidcock, E.; Rodriguez-Monge, L.; Taylor, R.; van de Streek, J.; Wood, P. A., Mercury CSD 2.0 - new features for the visualization and investigation of crystal structures. *J. Appl. Crystallogr.* **2008,** *41* (2), 466-470.
6. Das, S. K.; Frey, J., Regioselective double Boekelheide reaction: first synthesis of 3,6-dialkylpyrazine-2,5-dicarboxaldehydes from dl-alanine. *Tetrahedron Lett.* **2012,** *53* (30), 3869-3872.
7. Abudayyeh, A. M.; Schott, O.; Hanan, G. S.; Brooker, S., Copper catalysts for photo- and electro-catalytic hydrogen production. *Inorg. Chem. Front.* **2021,** *8*, 1015-1029.
8. Zanello, P., *Inorganic Electrochemistry: Theory, Practice and Application*. Royal Society of Chemistry: Cambridge, UK, 2003; p 615.
9. Appel, A. M.; Helm, M. L., Determining the Overpotential for a Molecular Electrocatalyst. *ACS Catal.* **2014,** *4* (2), 630-633.